Monthly Notices
of the
ROYAL ASTRONOMICAL SOCIETY

MNRAS **456,** 3743–3756 (2016) doi:10.1093/mnras/stv2935

Testing deviations from ΛCDM with growth rate measurements from six large-scale structure surveys at $z = 0.06$–1

Shadab Alam,[1,2]★ Shirley Ho[1,2] and Alessandra Silvestri[3]

[1] *Department of Physics, Carnegie Mellon University, 5000 Forbes Ave., Pittsburgh, PA 15217, USA*
[2] *McWilliams Center for Cosmology, Carnegie Mellon University, 5000 Forbes Ave., Pittsburgh, PA 15217, USA*
[3] *Institute Lorentz, Leiden University, PO Box 9506, NL-2300 RA Leiden, the Netherlands*

Accepted 2015 December 12. Received 2015 December 5; in original form 2015 September 27

ABSTRACT

We use measurements from the *Planck* satellite mission and galaxy redshift surveys over the last decade to test three of the basic assumptions of the standard model of cosmology, ΛCDM (Λ cold dark matter): the spatial curvature of the universe, the nature of dark energy and the laws of gravity on large scales. We obtain improved constraints on several scenarios that violate one or more of these assumptions. We measure $w_0 = -0.94 \pm 0.17$ (18 per cent measurement) and $1 + w_a = 1.16 \pm 0.36$ (31 per cent measurement) for models with a time-dependent equation of state, which is an improvement over current best constraints. In the context of modified gravity, we consider popular scalar–tensor models as well as a parametrization of the growth factor. In the case of one-parameter $f(R)$ gravity models with a ΛCDM background, we constrain $B_0 < 1.36 \times 10^{-5}$ (1σ C.L.), which is an improvement by a factor of 4 on the current best. We provide the very first constraint on the coupling parameters of general scalar–tensor theory and stringent constraint on the only free coupling parameter of Chameleon models. We also derive constraints on extended Chameleon models, improving the constraint on the coupling by a factor of 6 on the current best. The constraints on coupling parameter for Chameleon model rule out the value of $\beta_1 = 4/3$ required for $f(R)$ gravity. We also measure $\gamma = 0.612 \pm 0.072$ (11.7 per cent measurement) for growth index parametrization. We improve all the current constraints by combining results from various galaxy redshift surveys in a coherent way, which includes a careful treatment of scale dependence introduced by modified gravity.

Key words: gravitation – galaxies: statistics – cosmological parameters.

1 INTRODUCTION

Since its development a century ago, General Relativity (GR) has consistently provided a very successful framework to describe the evolution of our Universe (Peebles 1980; Davis & Peebles 1983). Nowadays, the prediction of GR for the growth of the large-scale structure that we observe around us is reaching great precision as cosmic microwave background (CMB) measurements are providing us with impressively accurate estimates of the cosmological parameters (Planck Collaboration 2015a). Yet, the excitement about the advances of observational cosmology is accompanied by the awareness that we face some major challenges. While the standard cosmological model, based on the laws of GR, provides a very good fit to existing data, it relies on a universe of which we understand only ∼5 per cent of the content. The remaining energy budget comes in the form of dark matter (∼27 per cent), responsible for the clustering of structure, and the cosmological constant Λ (Einstein 1915, ∼ 68 per cent), responsible for the phase of accelerated expansion recently entered by the universe. In particular, the physical understanding of cosmic acceleration represents one of the most important challenges in front of modern physics. While Λ is in good agreement with available data, e.g. baryon acoustic oscillations (BAO; Cole et al. 2005; Eisenstein et al. 2005; Hütsi 2006; Kazin et al. 2010; Percival et al. 2010; Reid et al. 2010; Anderson et al. 2014a,b; Aubourg et al. 2015), supernovae (SNe; Perlmutter & Schmidt 2003; Conley et al. 2011; Goobar & Leibundgut 2011; Suzuki et al. 2012; Rodney et al. 2014) and CMB (Planck Collaboration 2015a; *WMAP*9, Bennett et al. 2013) observations, it suffers from the coincidence and fine tuning problems (Weinberg 1989; Carroll 2001). Several alternatives to Λ have been proposed in the two decades since the discovery of cosmic acceleration (Riess et al.

★ E-mail: shadaba@andrew.cmu.edu

1998; Perlmutter et al. 1999), and they can be roughly divided into two classes. The first class, to which we will refer as *modified gravity* (MG), corresponds to modifications of the laws of gravity on large scales, designed to achieve self-accelerating solutions when matter becomes negligible (Silvestri & Trodden 2009; Clifton et al. 2012); alternatively, one can introduce a dynamical degree of freedom, commonly dubbed *dark energy* (DE; first coined by Huterer & Turner 1999), which is smoothly distributed and starts to dominate the evolution of the Universe at late times (Copeland, Sami & Tsujikawa 2006).

Undoubtedly, one of the important tasks for modern cosmologists is to perform precision tests of the standard model of cosmology (ΛCDM, Λ cold dark matter) and identify areas of tension. In a joint effort, one needs to also explore the parameter space of alternative models. Even though with the current constraints from data, any departure from ΛCDM is likely to be small and challenging to detect, we are in a unique position to test GR, and the other assumptions of ΛCDM, to unprecedented precision with modern observational probes. The three basic assumptions of ΛCDM which are popularly tested are the curvature of the universe, the nature of DE and the laws of gravitational interaction on large scales. The curvature of the universe can be explored by allowing a curvature density parameter, Ω_K, to be different from zero and free to vary. As for the nature of DE, we will focus on smoothly distributed models where it suffices to test for the deviation of the equation of state parameter, w, from -1, which is the value it assumes if the acceleration is driven by Λ. We will consider both a constant w and a time-dependent one, resorting to the popular Chevallier–Polarski–Linder (CPL) parametrization in terms of w_0 and w_a, i.e. $w = w_0 + w_a \frac{z}{1+z}$ (Chevallier & Polarski 2001; Linder 2003). Finally, we will explore the nature of gravity by replacing GR with various MG models, including Chameleon-type scalar–tensor theories and popular parametrizations of the growth rate. All these alternatives that we consider in our analysis affect, in one way or another, the rate at which large-scale structures grow. Models of smoothly distributed DE, which does not cluster, modify only the background dynamics of the universe, but this still has an impact on the rate at which structure forms. On the other hand, models of MG generally modify both the background and perturbation dynamics, leading to a significant effect on the growth rate.

Modern galaxy redshift surveys have successfully measured the growth rate using redshift space distortions (hereafter RSD; Kaiser 1987), which is the distortion induced in the galaxy correlation function by the peculiar velocity component of the galaxy redshift. Hence, on linear scales, RSD offers a handle both on the distribution of matter overdensity and peculiar velocity of galaxies. Recent galaxy redshift surveys have provided the measurement of $f\sigma_8(z)$ up to redshift $z = 0.8$, where f is the growth rate, i.e. the logarithmic derivative of the growth factor, and σ_8 is the rms amplitude of matter fluctuations in a sphere of radius 8 h^{-1} Mpc. In this paper, we will test all the three assumptions of ΛCDM listed above using the *Planck* CMB measurement (Planck Collaboration I 2014a) and latest RSD measurement from BOSS CMASS (Alam et al. 2015b), SDSS LRG (Samushia, Percival & Raccanelli 2012), 6dFGRS (Beutler et al. 2012), 2dFGRS (Percival et al. 2004), WiggleZ (Blake et al. 2011a) and VIMOS Public Extragalactic Redshift Survey (VIPERS; de la Torre et al. 2013). It is difficult to use the measurement from different surveys as they have different assumptions. We have looked into these assumptions and possible systematic while combining results from the different survey and also proposed a way to test scale dependence for MG models using these results.

2 THEORY

In exploring the power of RSD data to constrain deviations from the standard cosmological scenario, we consider several alternative models, divided into DE models that modify the background expansion history without introducing any clustering degree of freedom and those that instead modify only the dynamics of perturbations while keeping the background fixed to ΛCDM. In the former case, we consider one- and two-parameter extensions of the standard scenario, corresponding to different equations of state for DE or a non-zero spatial curvature. More specifically, we consider a wCDM universe, where the equation of state for DE is a constant parameter that can differ from the ΛCDM value $w = -1$; a (w_0, w_a)CDM universe, in which the equation of state for DE is a function of time and is approximation to exact solutions of the scalar field equation of motion, i.e. the CPL parametrization $w = w_0 + w_a(1 - a)$; a $o\Lambda$CDM universe which can have a spatial curvature different from zero, parametrized in terms of the corresponding fractional energy density Ω_K. In the case of models that modify the equations for the evolution of perturbations, we analyse Chameleon-type scalar–tensor theories, $f(R)$ gravity and a time-dependent parametrization of the growth rate.

We use the publicly available Einstein–Boltzmann solver MGCAMB (Hojjati, Pogosian & Zhao 2011)[1] to evolve the dynamics of scalar perturbations and obtain predictions to fit to our data set for all the models considered, except for the (w_0, w_a)CDM case. The latter needs to be treated instead through the PPF module (Fang, Hu & Lewis 2008) in CAMB.[2] While the implementation of the non-clustering DE models is trivial, in the following we shall describe in more detail the implementation of the MG models.

2.1 Scalar–tensor theories

Going beyond simple extensions of the standard model and non-clustering DE models, one needs to take into consideration also the modifications to the equations for cosmological perturbations. Given the cosmological probes that we consider in our analysis, it suffices for us to focus on linear scalar perturbations. In this context, it is possible to generally parametrize deviations from the standard cosmological scenario in the dynamics of perturbations by means of two functions of time and scale introduced in the set of Einstein and Boltzmann equations for metric and matter perturbations. More precisely, in the absence of anisotropic stress, one can write the Poisson and anisotropy equations as follows:

$$k^2\Psi = -\frac{a^2}{2M_P^2}\mu(a,k)\rho\Delta\,, \quad \frac{\Phi}{\Psi} = \gamma_{\rm slip}(a,k), \tag{1}$$

where $\rho\Delta \equiv \rho\delta + 3\frac{aH}{k}(\rho + P)v$ is the comoving density perturbation of matter fields and we have selected the conformal Newtonian gauge with Ψ and Φ representing the perturbation to, respectively, the time–time and space–space diagonal component of the metric. And then combine them with the unmodified Boltzmann equations for matter fields.

We shall focus on scalar–tensor theories where the metric and the additional scalar degree of freedom obey second-order equations of motion and will adopt the parametrization introduced in (Bertschinger & Zukin 2008, BZ) to describe the corresponding

[1] http://www.sfu.ca/aha25/MGCAMB.html
[2] http://camb.info

form of $(\mu, \gamma_{\rm slip})$, i.e.

$$\mu = \frac{1+\beta_1\lambda_1^2 k^2 a^s}{1+\lambda_1^2 k^2 a^s}\,,$$
$$\gamma_{\rm slip} = \frac{1+\beta_2\lambda_2^2 k^2 a^s}{1+\lambda_2^2 k^2 a^s} \qquad (2)$$

where we have adopted the convention of Zhao et al. (2009) and β_1, β_2 are dimensionless constants representing couplings, λ_1, λ_2 have dimensions of length and $s > 0$ to ensure that at early times GR is recovered. This parametrization gives a very good representation of scalar–tensor theories in the quasi-static regime, where time derivatives of the perturbations to the metric and scalar degree of freedom are neglected with respect to their spatial gradients on sub-horizon scales (Zhao et al. 2009; de Felice, Mukohyama & Tsujikawa 2010; Hojjati et al. 2012; Amendola et al. 2013; Silvestri, Pogosian & Buniy 2013). This is a good approximation given the observables that we are considering. Additionally, equation (2) sets the evolution of the characteristic length-scales of the models to a power law in the scale factor. This is of course a choice of parametrization for the time dependence of the mass scale of the scalar degree of freedom, and other choices are possible. Nevertheless, as we will discuss in the following, it is a good approximation for several scalar–tensor models, and data are not that sensitive to the specific choice of the time dependence.

Equations (2) are built-in in MGCAMB and allow us to easily extract predictions for scalar–tensor models on a ΛCDM background for different observables, including the growth rate.

2.2 Chameleon models

Chameleon models are a class of scalar–tensor theories for which the additional scalar field has a standard kinetic term and is conformally coupled to matter fields as follows:

$$S = \int {\rm d}^4x\sqrt{-\tilde{g}}\left[\frac{M_P^2}{2}\tilde{R} - \frac{1}{2}g^{\tilde{\mu}\nu}(\tilde{\nabla}_\mu\phi)\tilde{\nabla}_\nu\phi - V(\phi)\right] + S_i\left(\chi_i, {\rm e}^{-\kappa\alpha_i(\phi)}\tilde{g}_{\mu\nu}\right), \qquad (3)$$

where $\alpha_i(\phi)$ is the coupling between the scalar field ϕ and the ith matter species. The coupling(s) in general can be a non-linear function(s) of the field ϕ; however, since the value of the field ϕ typically does not change significantly on the time-scales associated with the epoch of structure formation, we will assume it to be linear in ϕ. Since we are dealing with clustering of matter in the late universe, it is safe to consider one coupling, i.e. to dark matter, that amounts to neglecting differences between baryons and dark matter, or simply neglecting baryons, which is safe for the observables under consideration.

In the quasi-static regime, $(\mu, \gamma_{\rm slip})$ for Chameleon-type theories can be well represented by a simplified version of equation (2) for which

$$1 + \frac{1}{2}\left(\frac{{\rm d}\alpha}{{\rm d}\phi}\right)^2 = \beta_1 = \frac{\lambda_2^2}{\lambda_1^2} = 2 - \beta_2\frac{\lambda_2^2}{\lambda_1^2}\,, \quad 1 \le s \le 4. \qquad (4)$$

Therefore, the effects of Chameleon-type theories on the dynamics of linear scalar perturbations on sub-horizon regimes can be described with good accuracy in terms of three parameters: $\{\beta_1, \lambda_1, s\}$. The last condition in equation (4) is broadly valid for models with runaway and tracking-type potentials (Zhao et al. 2009). Following a convention which is commonly used for $f(R)$ theories, let us express the length-scale λ_1^2 in terms of a new parameter B_0, which corresponds to the value of the inverse mass scale today in units of the horizon scale (Song, Hu & Sawicki 2007):

$$B_0 \equiv \frac{2H_0^2\lambda_1^2}{c^2}, \qquad (5)$$

so that we will work with $\{\beta_1, B_0, s\}$.

Let us notice that Chameleon theories as defined in action (equation 3) have necessarily $\beta_1 \ge 1$. However, in previous analysis of Chameleon models under the BZ parametrization, such theoretical prior has not been generally imposed and a wider range of β_1 has been explored (see e.g. Hojjati et al. 2011; Di Valentino et al. 2012). Hence, in our analysis we will consider both the case with $\beta_1 > 1$ and the case for which β_1 is allowed to be smaller than unity, to facilitate comparison. We will refer to the former as the *Chameleon* model, and the latter as the extended Chameleon model (*eChameleon*). We shall emphasize that we consider the eChameleon as a purely phenomenological model within equation (2), without linking it to action (equation 3), since it would not be viable case of the latter. While the eChameleon might correspond to a very special subcase of the parametrization (equation 2), it still represents a possible choice for $(\mu, \gamma_{\rm slip})$ and, as we will discuss in Section 6, it will be interesting to see what data can say about it.

2.3 *f*(*R*) gravity

$f(R)$ theories of gravity correspond to the simple modification of the Einstein–Hilbert action by the addition of a non-linear function of the Ricci scalar. In the past decade, they have been extensively explored as candidate models for cosmic acceleration (see e.g. Silvestri & Trodden 2009; de Felice et al. 2010 and references therein). They represent a subcase of the larger class of models described by action (equation 3), corresponding to a universal fixed coupling $\alpha_i = \sqrt{2/3}\,\phi$ and are therefore well represented in the quasi-static regime by the functions (2) and conditions (4). However, the fixed coupling $\alpha_i = \sqrt{2/3}\,\phi$ implies that $\beta_1 = 4/3$, and viable $f(R)$ models that closely mimic ΛCDM have been shown to correspond to $s \sim 4$ (Zhao et al. 2009; Hojjati et al. 2012). Therefore, the number of free parameters in equations (2) can be effectively reduced to λ_1, which is then expressed in terms of B_0. The latter is in fact the only free parameter needed to label the family of $f(R)$ models that reproduce a given expansion history, in our case the ΛCDM one, and can be usually reconstructed via the so-called designer approach (Song et al. 2007; Pogosian & Silvestri 2008). Alternatively, one could adopt the recently developed EFTCAMB package for an exact implementation of designer $f(R)$ models that does not rely on the quasi-static approximation (Hu et al. 2014; Raveri et al. 2014).[3] The latter method allows one to choose different background histories; however, for the data and cosmology involved in our analysis, MGCAMB provides enough accuracy.

2.4 Growth index parametrization of the growth rate

In the cosmological concordance model, as well as in non-clustering DE models, the growth rate of structure is well approximated by

$$f \equiv \frac{{\rm d}\ln\delta_{\rm m}}{{\rm d}\ln a} \approx \Omega_{\rm m}(a)^{6/11}, \qquad (6)$$

where $\Omega_{\rm m}(a) \equiv \rho_{\rm m}(a)/3M_P^2H^2(a)$, $\rho_{\rm m}$ is the background density of matter and $\delta_{\rm m} \equiv \delta\rho_{\rm m}/\rho_{\rm m}$. This inspired the following

[3] http://wwwhome.lorentz.leidenuniv.nl/~hu/codes/

Table 1. Measurement of $f(z)\sigma_8(z)$ from various galaxy redshift surveys covering redshift between 0.06 to 0.8.

z	$f\sigma_8(z)$	$1/k$ (h^{-1} Mpc)	Survey
0.067	0.42 ± 0.05	16.0–30	6dFGRS(2012)
0.17	0.51 ± 0.06	6.7–50	2dFGRS(2004)
0.22	0.42 ± 0.07	3.3–50	WiggleZ(2011)
0.25	0.35 ± 0.06	30–200	SDSS LRG (2011)
0.37	0.46 ± 0.04	30–200	SDSS LRG(2011)
0.41	0.45 ± 0.04	3.3–50	WiggleZ(2011)
0.57	0.462 ± 0.041	25–130	BOSS CMASS
0.6	0.43 ± 0.04	3.3–50	WiggleZ(2011)
0.78	0.38 ± 0.04	3.3–50	WiggleZ(2011)
0.8	0.47 ± 0.08	6.0–35	VIPERS(2013)

parametrization for deviations in the growth of structure (Wang & Steinhardt 1998; Linder 2005; Linder & Cahn 2007)

$$f = \Omega_{\rm m}(a)^{\gamma}, \tag{7}$$

where γ is commonly referred to as growth index (not to be confused with the $\gamma_{\rm slip}$ defined above, which represents instead the gravitational slip).

The idea behind this parametrization is that of capturing independently in $\Omega_{\rm m}$ and γ the information from, respectively, the expansion and the growth history. Since in our analysis we fix the background to ΛCDM, $\Omega_{\rm m}(a)$ is determined by that and the only parameter of interest will be γ. While for models of MG and clustering DE in general γ will be a function of time and scale, in several cases for the regime of interest it can still be safely approximated by a constant, which can differ significantly from the ΛCDM value. See Linder & Cahn (2007) for more details and some forms of γ in alternative theories of gravity.

In our analysis, we will assume that γ is constant and explore constraints on it after extracting predictions for the CMB and growth of structure from MGCAMB.

3 OBSERVATIONS

We use measurements of CMB angular power spectrum(C_l) from *Planck* 2013 (Planck Collaboration XV 2014b) combined with the measurement of $f(z)\sigma_8(z)$ from various redshift surveys covering between $z = 0.06$ and 0.8 listed in Table 1 as our main data points. Fig. 1 shows the measurements used with and without corrections and *Planck* 2013 prediction. We briefly describe each of the surveys and $f\sigma_8$ measurements in the following sections.

3.1 6dFGRS

The 6dFGRS (6 degree Field Galaxy Redshift Survey) has observed 125 000 galaxies in near-infrared band across 4/5th of southern sky (Jones et al. 2009). The surveys covers redshift range $0 < z < 0.18$, and has an effective volume equivalent to 2dFGRS (Percival et al. 2004) galaxy survey. The RSD measurement was obtained using a subsample of the survey consisting of 81 971 galaxies (Beutler et al. 2012). The measurement of $f\sigma_8$ was obtained by fitting 2D correlation function using streaming model and fitting range 16–30 Mpc h^{-1}. The Alcock–Paczynski (AP) effect (Alcock & Paczynski 1979) has been taken into account and it has a negligible effect (Beutler et al. 2012). The final measurement uses *Wilkinson Microwave Anisotropy Probe* 7 (*WMAP*7; Bennett et al. 2013) likelihood in the analysis. To be able to use this $f\sigma_8$ measurement, we need to account for the transformation to the *Planck* best-fitting cosmology (Planck Collaboration I 2014a).

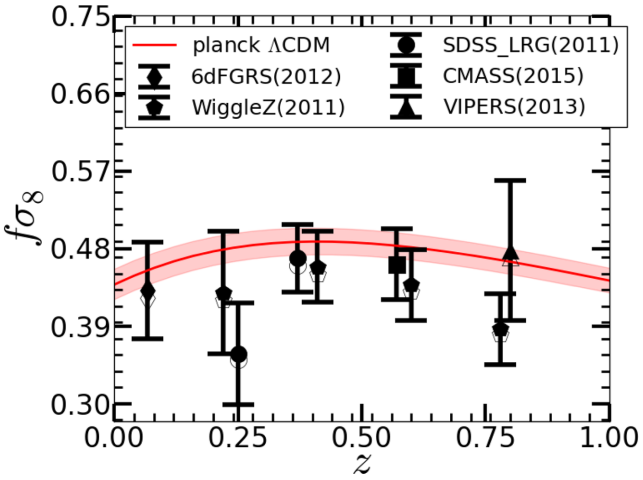

Figure 1. The measured $f\sigma_8$ from different surveys covering redshift range $0.06 < z < 0.8$. The empty markers represent the reported measurement of $f\sigma_8$ and the filled markers are for the corrected values for *Planck* cosmology. The red band shows the *Planck* ΛCDM 1σ prediction.

3.2 2dFGRS

The 2dFGRS (2 degree Field Galaxy Redshift Survey) obtained spectra for 221 414 galaxies in visible band on the southern sky (Colless et al. 2003). The survey covers redshift range $0 < z < 0.25$ and has an effective area of 1500 square degrees. The RSD measurement was obtained by linearly modelling the observed distortion after splitting the overdensity into radial and angular components (Percival et al. 2004). The parameters were fixed at different values $n_{\rm s} = 1.0$, $H_0 = 72$. The results were marginalized over power spectrum amplitude and $b\sigma_8$. We are not using this measurement in our analysis for two reasons. First, the survey has a huge overlap with 6dFGRS which will lead to a strong correlation between the two measurements. Secondly, the cosmology assumed is quite far from *WMAP*7 and *Planck* which may cause our linear theory approximation used to shift the cosmology to fail.

3.3 WiggleZ

The WiggleZ Dark Energy Survey is a large-scale galaxy redshift survey of bright emission line galaxies. It has obtained spectra for nearly 200 000 galaxies. The survey covers redshift range $0.2 < z < 1.0$, covering effective area of 800 square degrees of equatorial sky (Blake et al. 2011b). The RSD measurement was obtained using a subsample of the survey consisting of 152 117 galaxies. The final result was obtained by fitting the power spectrum using the Jennings, Baugh & Pascoli (2011) model in four non-overlapping slices of redshift. The measured growth rate is $f\sigma_8(z) = (0.42 \pm 0.07, 0.45 \pm 0.04, 0.43 \pm 0.04, 0.38 \pm 0.04)$ at effective redshift $z = (0.22, 0.41, 0.6, 0.78)$ with non-overlapping redshift slices of $z_{\rm slice} = ([0.1, 0.3], [0.3, 0.5], [0.5, 0.7], [0.7, 0.9])$, respectively. We can assume the covariance between the different measurements to be zero because they have no volume overlap.

3.4 SDSS LRG

The Sloan Digital Sky Survey (SDSS) Data Release 7 (DR7) is a large-scale galaxy redshift survey of luminous red galaxies (LRGs; Eisenstein et al. 2011). The DR7 has obtained spectra of 106 341 LRGs, covering 10 000 square degrees in redshift range $0.16 < z < 0.44$. The RSD measurement was obtained by modelling monopole and quadruple moment of galaxy auto-correlation function using linear theory. The data were divided in two redshift bins: $0.16 < z < 0.32$ and $0.32 < z < 0.44$. The measurements of growth rate are $f\sigma_8(z) = (0.3512 \pm 0.0583, 0.4602 \pm 0.0378)$ at effective redshift of 0.25 and 0.37, respectively (Samushia et al. 2012). These measurements are independent because there is no overlapping volume between the two redshift slices.

3.5 BOSS CMASS

SDSS Baryon Oscillation Spectroscopic Survey (BOSS; Dawson et al. 2013) targets high-redshift ($0.4 < z < 0.7$) galaxies using a set of colour–magnitude cuts. The growth rate measurement uses the CMASS (Reid et al. 2016; Anderson et al. 2014b) sample of galaxies from Data Release 11 (Alam et al. 2015a). The CMASS sample has 690 826 LRGs covering 8498 square degrees in the redshift range $0.43 < z < 0.70$, which correspond to an effective volume of 6 Gpc^3. The $f\sigma_8$ is measured by modelling the monopole and quadruple moment of galaxy auto-correlation using convolution Lagrangian perturbation theory (Carlson, Reid & White 2013) in combination with Gaussian streaming model (Wang, Reid & White 2014). The reported measurement of growth rate is $f\sigma_8 = 0.462 \pm 0.041$ at effective redshift of 0.57 (Alam et al. 2015b).

We are also using the combined measurement of growth rate ($f\sigma_8$), angular diameter distance (D_A) and Hubble constant (H) measured from the galaxy auto-correlation in CMASS sample at an effective redshift of 0.57 (Alam et al. 2015b). The measurement and its covariance are given below and it is called eCMASS,

$$f\sigma_8 = 0.46,\ D_A = 1401,\ H = 89.15$$
$$C_{\rm eCMASS} = \begin{pmatrix} 0.0018 & -0.6752 & -0.1261 \\ -0.6752 & 550.61 & 45.881 \\ -0.1261 & 45.881 & 14.019 \end{pmatrix}. \quad (8)$$

3.6 VIPERS

VIPERS (de la Torre et al. 2013) is a high-redshift small-area galaxy redshift survey. It has obtained spectra for 55 358 galaxies covering 24 square degrees in the sky from redshift range $0.4 < z < 1.2$. The measurement of growth factor uses 45 871 galaxies covering the redshift range $0.7 < z < 1.2$. The $f\sigma_8$ measurement is obtained by modelling the monopole and quadruple moments of galaxy auto-correlation function between the scale 6 and 35 h^{-1} Mpc. They have reported $f\sigma_8 = 0.47 \pm 0.08$ at effective redshift of 0.8. The perturbation theory used in the analysis has been tested against N-body simulation and shown to work at mildly non-linear scale below 10 h^{-1} Mpc (de la Torre et al. 2013).

3.7 *Planck* CMB

Planck is a space mission dedicated to the measurement of CMB anisotropies. It is the third generation of all sky CMB experiment following *COBE* and *WMAP*. The primary aim of the mission is to measure the temperature and polarization anisotropies over the entire sky. The *Planck* mission provides a high-resolution map of CMB anisotropy which is used to measure the cosmic variance-limited angular power spectrum C_ℓ^{TT} at the last scattering surface. The *Planck* measurements help us constrain the background cosmology to unprecedented precision (Planck Collaboration I 2014a; Planck Collaboration XVI 2014c; Planck Collaboration 2015a). We are using the CMB measurements from *Planck* satellite in order to constrain cosmology. We have assumed that *Planck* measurements are independent of the measurement of growth rate from various galaxy redshift surveys.

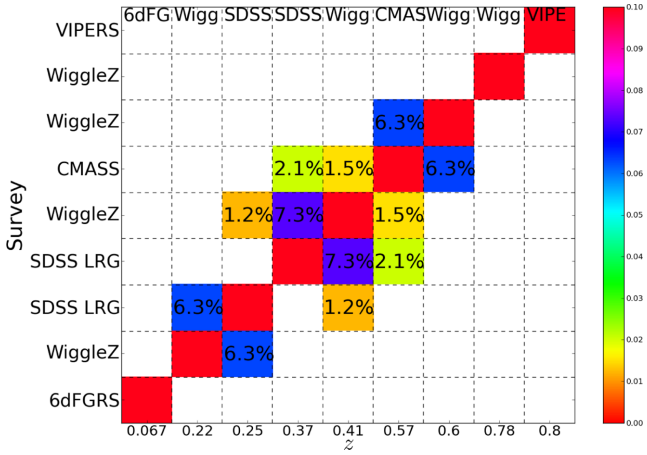

Figure 2. Correlation matrix between all the measurements used in our analysis. We have estimated the correlation as the fraction of overlap volume between two surveys to the total volume of the two surveys combined.

3.8 Correlation matrix

We use the measurements of $f\sigma_8$ from six different surveys. Although these surveys are largely independent, and in some cases they probe different biased tracers, they are measuring inherently the same matter density field. Therefore, the parts of the survey observing the same volume of sky cannot be treated as independent. We have predicted an upper limit to the overlap volume using the data from different surveys. We have estimated the fractional overlap volume between any two samples as the ratio of the overlap volume to the total volume of the two samples. We estimate the correlation between two measurements as the fractional overlap volume between the two measurements. Fig. 2 shows our estimate of the correlation between the surveys. The four measurements of WiggleZ survey cover the redshift range between 0.1 and 0.9 and hence show most correlation with other measurements like SDSS LRG and CMASS in the same redshift range.

4 POTENTIAL SYSTEMATICS

The collection of $f\sigma_8$ data points that we are using in this analysis contains measurements from several different surveys, obtained during the last decade, each with a different pipeline. Furthermore, often the latter implicitly assumes a GR modelling, which does not take into account the different predictions for the growth factor in modified theories of gravity. It is important to account for some crucial differences in order to use these measurements in our analysis. We have looked at following different aspects of measurements and theoretical prediction before using them in our analysis.

4.1 Fiducial cosmology of the growth rate ($f\sigma_8$)

The measurements of $f\sigma_8$ have been obtained over the time when we had transition from *WMAP* best-fitting cosmology (Hinshaw et al. 2013) to the *Planck* best-fitting cosmology (Planck Collaboration I 2014a). Since we are using *Planck* likelihood (Planck Collaboration XV 2014b) in our analysis, we have decided to convert all the measurements to *Planck* cosmology. The three-dimensional correlation function can be transformed from *WMAP* to the *Planck* cosmology using AP effect (Alcock & Paczynski 1979),

$$\xi_{\rm Planck}(r_\parallel, r_\perp, \phi) = \xi_{\rm WMAP}(\alpha_\parallel r_\parallel, \alpha_\perp r_\perp, \phi), \tag{9}$$

where $\alpha_\parallel$ is the ratio of the Hubble parameters ($\alpha_\parallel = H_{\rm Planck}/H_{\rm WMAP}$) and $\alpha_\perp$ is the ratio of the angular diameter distances ($\alpha_\perp = D_{\rm A}^{\rm WMAP}/D_{\rm A}^{\rm Planck}$). The $r_\parallel, r_\perp$ are pair separations along the line of sight and perpendicular to the line of sight, and ϕ is the angular position of pair separation vector in the plane perpendicular to the line of sight from a reference direction. In practice, the correlation function is isotropic along ϕ. We can calculate the corresponding power spectrum by applying Fourier transform to correlation function,

$$P_{\rm Planck}(k_\parallel, k_\perp, k_\phi) = \int {\rm d}r_\parallel dr_\perp r_\perp d\phi \xi_{\rm Planck}(r_\parallel, r_\perp, \phi) {\rm e}^{-{\rm i}\boldsymbol{k}.\boldsymbol{r}} \tag{10}$$

$$= \int {\rm d}r'_\parallel dr'_\perp \frac{r'_\perp}{\alpha_\parallel \alpha_\perp^2} \xi_{\rm WMAP}(r'_\parallel, r'_\perp, \phi) {\rm e}^{-{\rm i}\boldsymbol{k}'.\boldsymbol{r}'} \tag{11}$$

$$= \frac{P_{\rm WMAP}(k_\parallel/\alpha_\parallel, k_\perp/\alpha_\perp, k_\phi)}{\alpha_\parallel \alpha_\perp^2}. \tag{12}$$

The Kaiser formula for RSD gives the redshift space correlation function as $P_g^s(k,\mu) = b^2 P_m(k)(1+\beta\mu^2)^2$ (Kaiser 1987). Using the linear theory Kaiser prediction and the above approximation between *WMAP* and *Planck* power spectrum, we can get a relation to transform the growth function from *WMAP* to *Planck* cosmology,

$$\frac{1+\beta_{\rm Planck}\mu'^2}{1+\beta_{\rm WMAP}\mu^2} = C\sqrt{\frac{P_{\rm Planck}(k',\mu')}{P_{\rm WMAP}(k,\mu)}} \tag{13}$$

$$= C\sqrt{\frac{1}{\alpha_\parallel \alpha_\perp^2}}, \tag{14}$$

where C is the ratio of isotropic matter power spectrum with *WMAP* and *Planck* cosmology integrated over scale used in β measurement,

$$C = \int_{k_1}^{k_2} {\rm d}k \sqrt{\frac{P^m_{\rm WMAP}(k)}{P^m_{\rm Planck}(k')}}, \tag{15}$$

with $k'_{(\parallel,\perp)} = k_{(\parallel,\perp)}/\alpha_{(\parallel,\perp)}$. When the right-hand side of equation (14) is close to 1, then we can approximate the above equation as follows:

$$\beta_{\rm Planck} = \beta_{\rm WMAP} C \frac{\mu^2}{\mu'^2}\sqrt{\frac{1}{\alpha_\parallel \alpha_\perp^2}}. \tag{16}$$

The ratio $\frac{\mu^2}{\mu'^2}$ can be obtained using simple trigonometry which gives following equations, where the last equation is approximation for $\alpha_\parallel^2 \approx \alpha_\perp^2$,

$$\frac{\mu^2}{\mu'^2} = \frac{1}{\alpha_\perp^2}\left(\alpha_\parallel^2 + (\alpha_\perp^2 - \alpha_\parallel^2)\mu^2\right) \approx \left(\frac{\alpha_\parallel}{\alpha_\perp}\right)^2. \tag{17}$$

We can substitute equation (17) in equation (16) in order to get the required scaling for f (growth factor) assuming that bias measured is proportional to the σ_8 of the cosmology used,

$$\beta_{\rm Planck} = \beta_{\rm WMAP} C \left(\frac{\alpha_\parallel}{\alpha_\perp^2}\right)^{(3/2)} \tag{18}$$

$$f\sigma_{8\,\rm Planck} = f\sigma_{8\,\rm WMAP} C \left(\frac{\alpha_\parallel}{\alpha_\perp^2}\right)^{(3/2)} \left(\frac{\sigma_8^{\rm Planck}}{\sigma_8^{\rm WMAP}}\right)^2. \tag{19}$$

We have tested prediction of equation (19) against the measurement of $f\sigma_8$ reported in table 2 of Alam et al. (2015b) at redshift 0.57 using both *Planck* and *WMAP* cosmology. In principle, the bias in the measurements of $f\sigma_8$ should be corrected for the each step of MCMC to the chosen cosmology. But, we choose not to incorporate that and apply only an overall correction. Because the corrections are negligible compared to the error on measurements.

4.2 Scale dependence

GR predicts a scale-independent growth factor. One of the important features of the MG theories we are considering is that they predict a scale-dependent growth factor which has a transition from high to low growth at certain scale which depends on the redshift z and the model parameters. The measurements we use from the different surveys assume a scale-independent $f\sigma_8$ and uses characteristic length-scale while analysing data. In order to account for all these effects, we have done our analysis in two different ways. In the first method, we assume that the measurements correspond to an effective k and in the second method, we treat the average theoretical prediction over range of k used in $f\sigma_8$ analysis.

Figs 11 and 12 show the parameter constraint for Chameleon models and $f(R)$ gravity. The grey and red contours result from using two different model predictions to test the scale dependence. The grey contours correspond to the model where we average $f\sigma_8$ over k used in respective $f\sigma_8$ analysis and red contours correspond to $f\sigma_8$ evaluated at $k = 0.2\,h\,{\rm Mpc}^{-1}$. It is evident from the plots that, at the current level of uncertainty, we obtain very similar constraint and hence do not detect any significant effect of scale dependence of $f\sigma_8$.

4.3 Other systematics

The measurements of $f\sigma_8$ are reported at the mean redshift of the surveys. But the galaxies used have a redshift distribution which in principle can be taken into account by integrating the theoretical prediction. This should be a very small effect because the $f\sigma_8(z)$ is relatively smooth and flat (see Fig. 1 and Huterer et al. 2015) for the redshift range of the survey and also because the survey window for every individual measurement is small. Another important point is the assumption of GR-based modelling for the measurement. We have looked at the modelling assumption for each of the measurements. All measurements of $f\sigma_8$ except WiggleZ and VIPERS allow the deviation from GR through AP effect (Alcock & Paczynski 1979) which justifies our use of *MG* models. The inclusion of AP in WiggleZ and VIPERS will marginally increase the error on the measurements. Different surveys use different ranges of scale in the RSD analysis. This will be important especially while analysing *MG* models. To account for the different scales used, we evaluate the prediction for each survey averaged over the scale used in the respective analysis.

5 ANALYSIS

We have measurement of $f\sigma_8$ from various surveys covering redshift range 0.06–0.8 (see Table 1). We first correct these measurements for the shift from *WMAP* cosmology to *Planck* cosmology as described in Section 4.1. The next step is to evaluate prediction from different MG theories by evolving a full set of linear perturbation equations. The theoretical predictions for $f\sigma_8$ are generally scale and redshift dependent (see Section 4.2). Therefore, we consider two cases for theoretical prediction: (1) evaluate $f\sigma_8$ at effective k and (2) evaluate $f\sigma_8$ averaged over range of k used in measurements. We also predict C_l^{TT} for different MG theories. Finally, we define our likelihood, which consists of three parts, one by matching *Planck* temperature fluctuation C_l^{TT}, second by matching growth factor from Table 1 and third by using eCMASS data as shown in equation (8). Therefore, we define the likelihood as follows:

$$\mathcal{L} = \mathcal{L}_{\rm Planck}\mathcal{L}_{f\sigma_8}\mathcal{L}_{\rm eCMASS} \tag{20}$$

$$\mathcal{L}_{f\sigma_8} = {\rm e}^{-\chi^2_{f\sigma_8}/2} \tag{21}$$

$$\chi^2_{f\sigma_8} = \Delta f\sigma_8 C^{-1}\Delta f\sigma_8^T. \tag{22}$$

The $\Delta f\sigma_8$ is the deviation of the theoretical prediction from the measurement and C^{-1} is the inverse of covariance which has diagonal error for different surveys and correlation between measurement as described in Section 3.8. Note that we do not include $f\sigma_8$ from CMASS while using eCMASS with $f\sigma_8(z)$ to avoid double counting. This likelihood is sampled using modified version of COSMOMC (Lewis & Bridle 2002; Hojjati et al. 2011). We sample over 6 cosmology parameters $\{\Omega_{\rm b}h^2, \Omega_{\rm c}h^2, 100\Theta_{\rm MC}, \tau, n_{\rm s}, \log(10^{10}A_{\rm s})\}$ and all 18 *Planck* nuisance parameters as described in Planck Collaboration I (2014a) with the respective extension parameters or MG parameters. The priors we have used on all the parameters are the same as the priors in Planck Collaboration I (2014a), and the priors we used on the parameters of MG model are given in Table 2.

6 RESULTS

We have combined CMB data set and measurements of growth from various redshift surveys in order to constrain the parameters of standard cosmology (ΛCDM), extended cosmology models and *MG*. Our analysis gives consistent constraints for the standard ΛCDM parameters $\{\Omega_{\rm b}h^2, \Omega_{\rm c}h^2, 100\Theta_{\rm MC}, \tau, n_{\rm s}, \log(10^{10}A_{\rm s})\}$ as shown in Table 3. Fig. 3 shows the constraint on $\Omega_{\rm m}$–σ_8 plane for ΛCDM, wCDM, $o\Lambda$CDM, scalar–tensor model, Chameleon gravity, eChameleon, $f(R)$ and growth index parametrization. These are our best constraints obtained using *Planck* +eCMASS + $f\sigma_8(z)$. Fig. 4 shows the theoretical predictions of $f\sigma_8(z)$ for each of the models considered in this paper.

6.1 ΛCDM

Fig. 5 shows the one-dimensional marginalized likelihood for standard ΛCDM cosmology. The black line shows the constraints from *Planck* 2013 alone. The red, blue and magenta lines are posterior obtained for the data set combinations *Planck*+eCMASS, *Planck*+$f\sigma_8(z)$ and *Planck*+eCMASS+$f\sigma_8(z)$, respectively. Our parameter constraints are completely consistent with the *Planck* 2013 results. Adding measurements of the growth rate to *Planck* data does not improve the results (see Fig. 5) due to already tight constraints from *Planck* observations (see Fig. 1).

Table 2. The list of extension parameters for all the models used in our analysis. For each parameter, we provide their symbol, prior range, central value and 1σ error.

Model	Parameter	Prior range	Posterior
wCDM	w_0	-2.0 to 0.0	-0.873 ± 0.077
w_0w_aCDM	w_0	-2.0 to 0.0	-0.943 ± 0.168
	w_a	-4.0 to 4.0	0.156 ± 0.361
$o\Lambda$CDM	Ω_k	-1.0 to 1.0	-0.0024 ± 0.0032
Scalar–tensor	β_1	0 to 2.0	1.23 ± 0.29
	β_2	0 to 2.0	0.93 ± 0.44
	$\lambda_1^2 \times 10^{-6}$	0 to 1	0.49 ± 0.29
	$\lambda_2^2 \times 10^{-6}$	0 to 1	0.41 ± 0.28
	s	1.0 to 4.0	2.80 ± 0.84
Chameleon	β_1	1.0 to 2.0	<1.008
	B_0	0 to 1.0	<1.0
	s	1.0 to 4.0	$2.27 < s < 4.0$
eChameleon	β_1	0 to 2.0	0.932 ± 0.031
	B_0	0 to 1.0	<0.613
	s	1.0 to 4.0	$2.69 < s < 4.0$
$f(R)$	B_0^a	10^{-10} to 10^{-4}	$<1.32 \times 10^{-5}$
Growth index	γ	0.2 to 0.8	0.611 ± 0.072

[a]We have tried using both logarithmic and linear prior on B_0 for the $f(R)$ model and obtained similar results for the upper limit on B_0. But, our final results are obtained using logarithmic prior on B_0 because the linear prior never converged due to huge range and strong constraint.

6.2 DE equation of state (wCDM)

We have looked at the wCDM, i.e. the one-parameter extension of ΛCDM where the DE equation of state is a constant, w. Fig. 6 shows the two-dimensional likelihood of w_0 and $\Omega_{\rm m}$. The grey contours are *Planck*-only constraint ($w_0 = -1.27 \pm 0.42$), red contours are *Planck* and eCMASS ($w_0 = -0.92 \pm 0.10$) and blue contours show *Planck* combined with eCMASS and growth factor measurements ($w_0 = -0.87 \pm 0.077$). We obtain $w_0 = -0.87 \pm 0.077$ (8.8 per cent measurement) which is consistent with the fiducial value of $w = -1$ for ΛCDM. The constraint we obtained is similar in precision as compared to BAO only, but has different degeneracy. Therefore, combined measurement of growth rate and anisotropic BAO for all of these surveys will help us improve the precision of w_0.

6.3 Time-dependent DE (w_0w_aCDM)

The wCDM model which proposes a constant DE is limited in its physical characteristics. Many models propose time-dependent DE which is popularly tested using linear relation $w(z) = w_0 + w_a\frac{z}{1+z}$, with w_0 and w_a as free parameters. This model has been shown to match exact solutions of distance, Hubble, growth to the 10^{-3} level of accuracy (de Putter & Linder 2008) for a wide variety of scalar field (and *MG*) models. The dynamical evolution of $w(z)$ can change the growth factor significantly and leave an imprint on the CMB. The combination of CMB and collection of growth factor at different redshifts is a unique way to test the time-dependent DE model.

Fig. 7 shows the 1σ and 2σ region for (w_0, w_a). The grey contour is from the *Planck* temperature power spectrum data alone

Table 3. The list of standard ΛCDM parameters used in our analysis. For each parameter, we provide its symbol, prior range, central value and 1σ error. We have used the same prior as *Planck* 2013 on these parameters. We have also marginalized over all the nuisance parameters of *Planck* likelihood. We report the results for each of the models analysed in this paper.

Models	$\Omega_b h^2$	$\Omega_c h^2$	$100\theta_{MC}$	τ	n_s	$\ln(10^{10}A_s)$
Prior range	0.005–0.10	0.001–0.99	0.50–10.0	0.01–0.8	0.9–1.1	2.7–4.0
ΛCDM	0.0219 ± 0.0002	0.1208 ± 0.0020	1.0410 ± 0.0006	0.0442 ± 0.0236	0.953 ± 0.0068	3.0007 ± 0.0450
wCDM	0.0221 ± 0.0003	0.1183 ± 0.0028	1.0414 ± 0.0006	0.0911 ± 0.0449	0.9615 ± 0.0097	3.0884 ± 0.0843
w_0w_aCDM	0.0221 ± 0.0003	0.1181 ± 0.0029	1.0415 ± 0.0007	0.0906 ± 0.0454	0.9619 ± 0.0099	3.0871 ± 0.0850
oΛCDM	0.0220 ± 0.0003	0.1191 ± 0.0031	1.0413 ± 0.0007	0.0518 ± 0.0278	0.9582 ± 0.0094	3.0118 ± 0.0514
Scalar–tensor	0.0221 ± 0.0003	0.1199 ± 0.0020	1.0412 ± 0.0006	0.0333 ± 0.0198	0.9591 ± 0.0071	2.9769 ± 0.0377
Chameleon	0.0219 ± 0.0002	0.1205 ± 0.0020	1.0411 ± 0.0006	0.0390 ± 0.0222	0.9539 ± 0.0067	2.9894 ± 0.0425
eChameleon	0.0218 ± 0.0003	0.1222 ± 0.0023	1.0409 ± 0.0006	0.1313 ± 0.0467	0.9537 ± 0.0079	3.1780 ± 0.0914
$f(R)$	0.0221 ± 0.0004	0.1182 ± 0.0033	1.0414 ± 0.0008	0.0733 ± 0.0354	0.9607 ± 0.0101	3.0526 ± 0.0663
Growth index (γ)	0.0218 ± 0.0003	0.1214 ± 0.0023	1.0409 ± 0.0006	0.0699 ± 0.0400	0.9525 ± 0.0075	3.0534 ± 0.0788

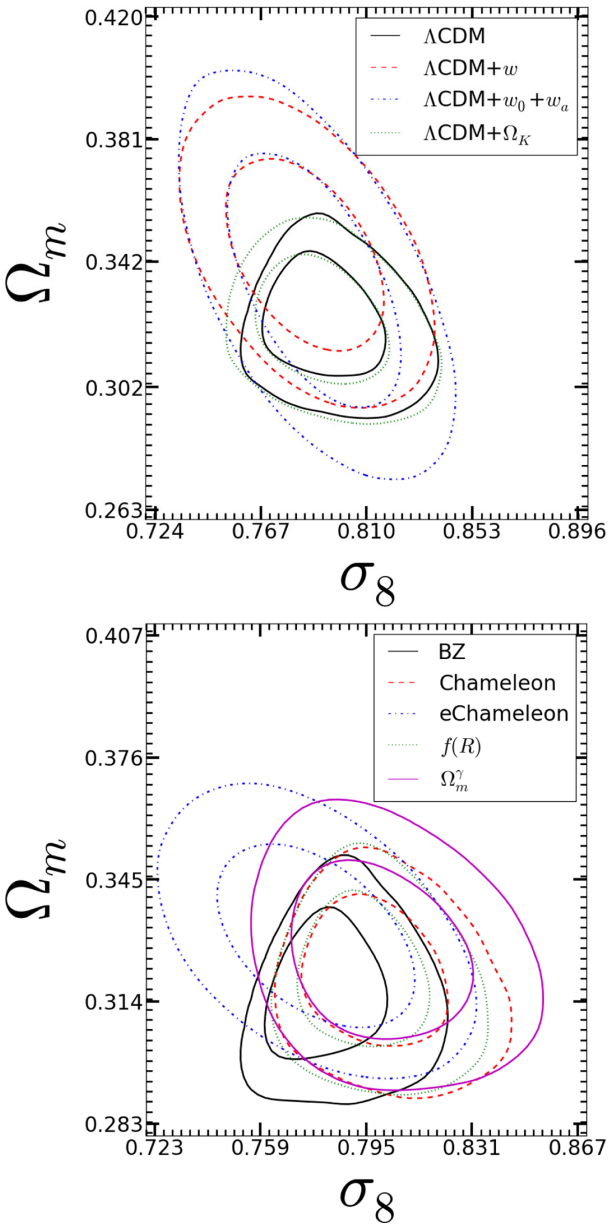

Figure 3. The 1σ and 2σ regions for each of the models considered in this paper in the Ω_m–σ_8 plane. It shows that the posterior likelihood is consistent for each of the models in this parameter space. The top plot shows the models which are extension to ΛCDM and the bottom plot shows the *MG* models.

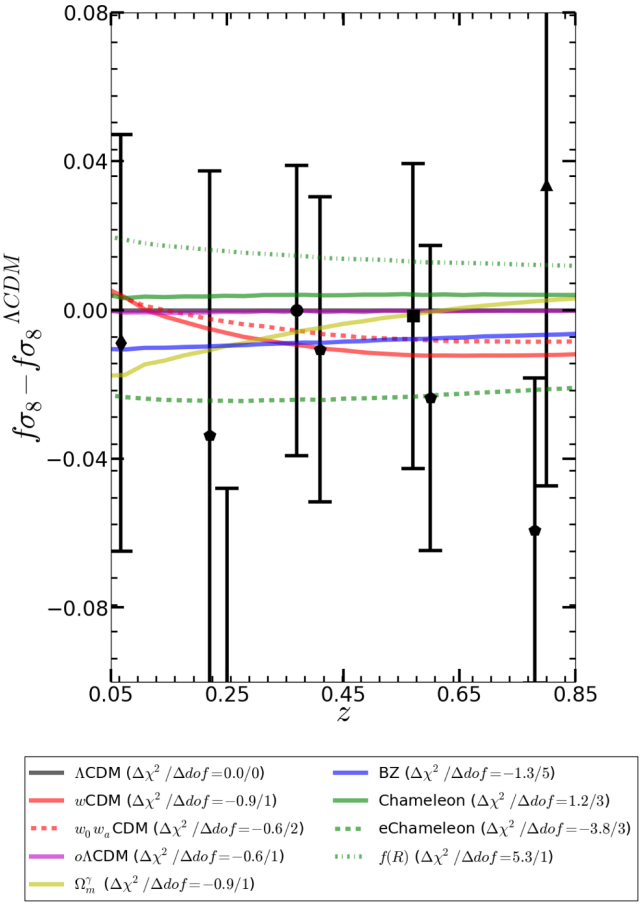

Figure 4. The black points show the corrected $f\sigma_8$ used in our analysis, along with the error bar. Lines of different colours show the best fit for the various models used in our analysis. The best fit and χ^2 are for the case of *Planck* $+f\sigma_8$ + eCMASS fits. Notice that the eChameleon model predicts the smallest growth rate by preferring lower values of the coupling constant (β_1), even though the scalar amplitude of primordial power spectrum is high.

($w_0 = -0.99 \pm 0.52$, $w_a = -1.50 \pm 1.46$). The red contours are from *Planck* and eCMASS ($w_0 = -1.23 \pm 0.26$, $w_a = 0.63 \pm 0.49$) and blue contour shows *Planck* combined with eCMASS and growth factor measurement ($w_0 = -0.94 \pm 0.17$, $w_a = 0.16 \pm 0.36$). The ΛCDM prediction of $(w_0, w_a) = (-1, 0)$ is completely consistent with our posterior. We have obtained constraint on $w_0 = -0.94 \pm 0.17$ (18 per cent measurement) and $1 + w_a = 1.16 \pm 0.36$ (31 per cent measurement) which is stronger constraint than

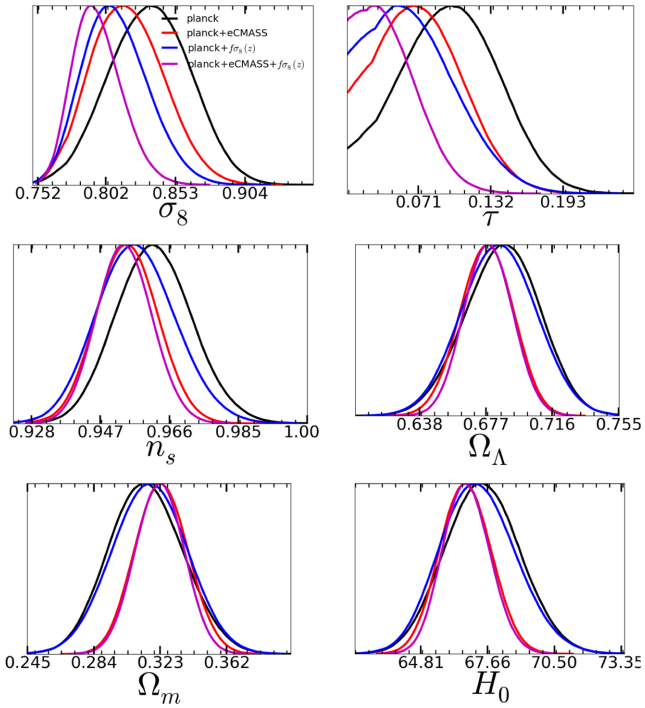

Figure 5. ΛCDM: we use GR as the model for gravity to determine the growth factor and fit for $f\sigma_8(z)$ and eCMASS measurement with *Planck* likelihood. The black line shows the constraints from *Planck* 2013 alone. The red, blue and magenta lines are posterior obtained for the data set combinations *Planck*+eCMASS, *Planck*+$f\sigma_8(z)$ and *Planck*+eCMASS+$f\sigma_8(z)$, respectively. The two most prominent effects are in optical depth τ and scalar amplitude of primordial power spectrum A_s, which is also reflected in the derived parameter σ_8 and mid-redshift of reionization z_{re}.

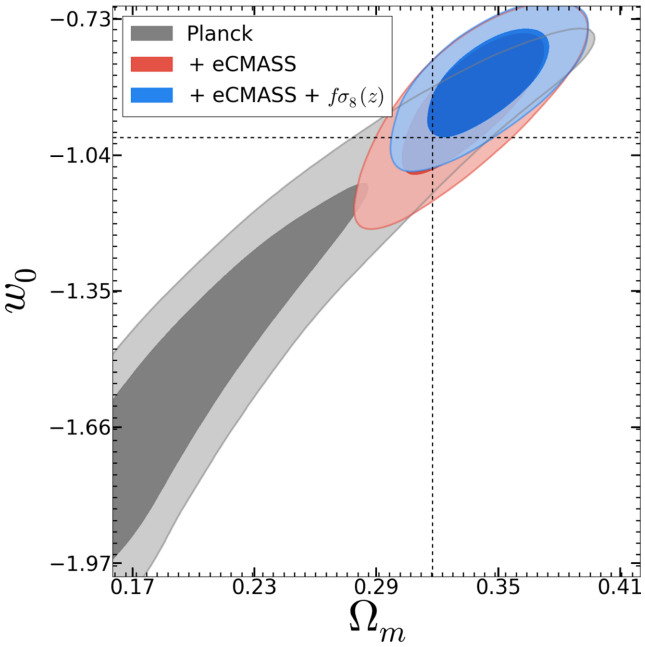

Figure 6. wCDM: the two-dimensional posterior likelihood w and Ω_m for wCDM. The grey contour is for *Planck* ($w_0 = -1.27 \pm 0.42$); red contour is combined constraint from *Planck* and eCMASS ($w_0 = -0.92 \pm 0.10$). The blue contour represents constraint from combining *Planck* with eCMASS and $f\sigma_8(z)$ ($w_0 = -0.87 \pm 0.077$).

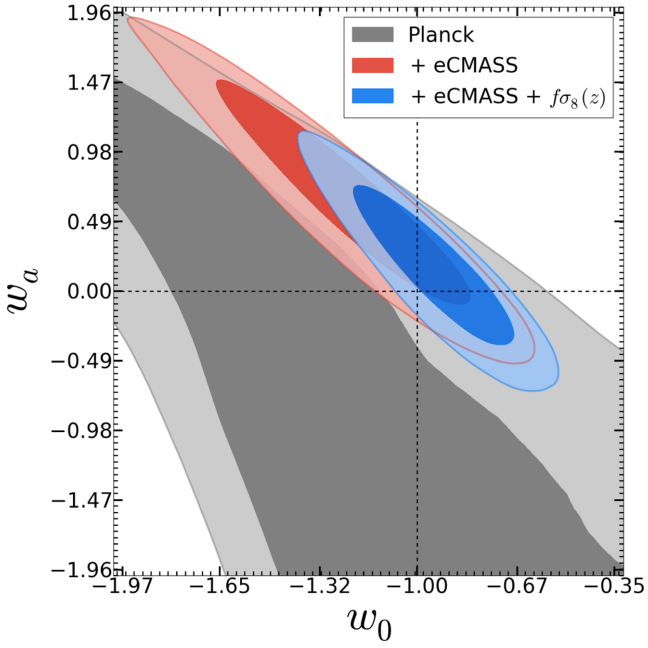

Figure 7. w_0w_aCDM: the two-dimensional posterior likelihood of w_0 and w_a for time-dependent DE model. The grey contour is for *Planck* ($w_0 = -0.99 \pm 0.52$, $w_a = -1.50 \pm 1.46$); red contour is combined constraint from *Planck* and eCMASS ($w_0 = -1.23 \pm 0.26$, $w_a = 0.63 \pm 0.49$). The blue contour represents results from combining *Planck* with eCMASS and $f\sigma_8(z)$ ($w_0 = -0.94 \pm 0.17$, $w_a = 0.16 \pm 0.36$).

the current best measurement of $w_a = -0.2 \pm 0.4$ from Aubourg et al. (2015).

6.4 Spatial curvature (*o*ΛCDM)

We consider a model with spatial curvature parametrized with Ω_K as free parameter called *o*ΛCDM along with ΛCDM parameters. Fig. 8 shows the posterior for the Ω_K and Ω_m plane. The grey contour is from the *Planck* temperature power spectrum data alone ($\Omega_k = -0.060 \pm 0.047$). The red contours are from *Planck* and eCMASS ($\Omega_k = -0.0024 \pm 0.0034$) and blue contour shows *Planck* combined with eCMASS and growth factor measurements ($\Omega_k = -0.0024 \pm 0.0032$). The ΛCDM prediction of $\Omega_k = 0$ is completely consistent with our posterior. We have obtained constraint on $1 + \Omega_k = 0.9976 \pm 0.0032$ (0.3 per cent measurement) which is competitive with the current best measurements (Aubourg et al. 2015). It will be interesting to see if combined RSD and BAO at all redshifts will give any improvement on the precision of curvature.

6.5 Scalar–tensor gravity (BZ parametrization)

The general scalar–tensor theories of gravity are analysed using five-parameter model called BZ parametrization. The five parameters of scalar–tensor gravity (β_1, β_2, λ_1, λ_2, s) are constrained along with the standard ΛCDM parameters using *Planck*, $f\sigma_8(z)$ and eCMASS measurements. BZ model predicts a scale-dependent growth rate ($f\sigma_8(k, z)$), whereas the measurements are at some effective k. In order to incorporate the k-dependence in our analysis, we use the two different approaches described in Section 4.2. Fig. 9 shows two-dimensional posterior in the plane (β_1, β_2). The green contour is combined constraint from *Planck* and eCMASS ($\beta_1 = 1.18 \pm 0.29$, $\beta_2 = 0.95 \pm 0.43$). The grey contour is the combined constraint from *Planck* and $f\sigma_8(z)$ with averaged over k ($\beta_1 = 1.24 \pm 0.3$,

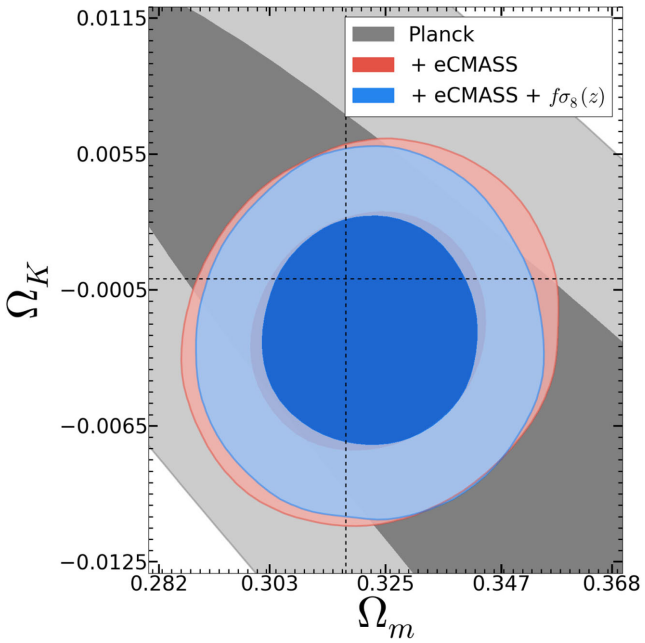

Figure 8. $o\Lambda$CDM: the two-dimensional posterior likelihood of Ω_k and Ω_m for $o\Lambda$CDM. The grey contour is for *Planck* ($\Omega_k = -0.060 \pm 0.047$); red contour is combined constraint from *Planck* and eCMASS ($\Omega_k = -0.0024 \pm 0.0034$). The blue contour represents results from combining *Planck* with eCMASS and $f\sigma_8(z)$ ($\Omega_k = -0.0024 \pm 0.0032$).

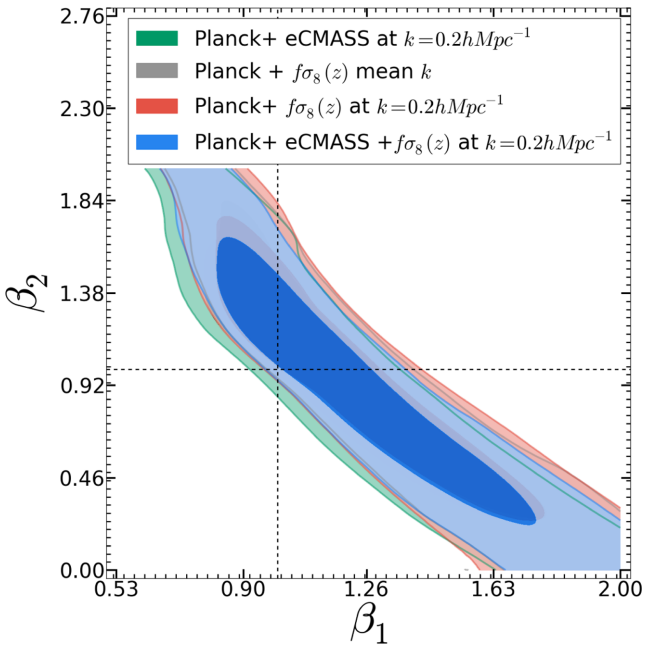

Figure 9. BZ: the two-dimensional posterior likelihood of β_1–β_2 for five-parameter scalar–tensor theory parametrized through the BZ form of equation (2). The green contour is the combined constraint from *Planck* and eCMASS ($\beta_1 = 1.18 \pm 0.29$, $\beta_2 = 0.95 \pm 0.43$). The grey contour is the combined constraint from *Planck* and $f\sigma_8(z)$ with averaged over k ($\beta_1 = 1.24 \pm 0.3$, $\beta_2 = 0.96 \pm 0.45$); red contour is the combined constraint from *Planck* and $f\sigma_8(z)$ at effective $k = 0.2\,h$ Mpc^{-1} ($\beta_1 = 1.24 \pm 0.3$, $\beta_2 = 0.95 \pm 0.45$). The blue contour represents results from the combination of *Planck*, $f\sigma_8(z)$ and eCMASS ($\beta_1 = 1.23 \pm 0.29$, $\beta_2 = 0.93 \pm 0.44$).

$\beta_2 = 0.96 \pm 0.45$); the red contour is the combined constraint from *Planck* and $f\sigma_8(z)$ at effective $k = 0.2\,h$ Mpc^{-1} ($\beta_1 = 1.24 \pm 0.3$, $\beta_2 = 0.95 \pm 0.45$). The blue contour represents results from the combination of *Planck*, $f\sigma_8(z)$ and eCMASS ($\beta_1 = 1.23 \pm 0.29$, $\beta_2 = 0.93 \pm 0.44$). We obtain the following joint constraint on the five BZ parameters: $\beta_1 = 1.23 \pm 0.29$, $\beta_2 = 0.93 \pm 0.44$, $\lambda_1^2(\times 10^{-6}) = 0.49 \pm 0.29$, $\lambda_2^2(\times 10^{-6}) = 0.41 \pm 0.28$ and $s = 2.80 \pm 0.84$. By looking at the joint 2D likelihood for (β_1, β_2) in Fig. 9, we notice that there is a strong degeneracy between the two parameters which reflects the degeneracy between μ and γ for the observables that we are using. Similar results have been found in Hojjati et al. (2012) and Planck Collaboration (2015b). For the next models that we will discuss, β_1 and β_2 are not independent and this will allow data to place more stringent constraints.

While the constraints on the length-scale of the scalar field (λ_1, λ_2) and (s) are very broad, the one on the coupling, β_1 and β_2, is the first ever constraint obtained on these parameters for general scalar–tensor gravity. The discrepancy in the strength of the constraints on the coupling and on the length-scale can be linked to the fact that data strongly prefer values of the coupling constants close to 1. For such values, the scale and time dependences in (μ, γ) become less important and therefore are loosely constrained. We will encounter this again in the Chameleon and $f(R)$ gravity cases.

6.6 Chameleon gravity

The three parameters of Chameleon gravity (β_1, B_0, s) are constrained along with the standard ΛCDM parameters using *Planck*, $f\sigma_8(z)$ and eCMASS measurements. Chameleon models predict a scale-dependent growth rate ($f\sigma_8(k, z)$), whereas the measurements are at some effective k. In order to incorporate the k-dependence in our analysis, we use the two different approaches described in Section 4.2. Fig. 10 shows the two-dimensional posterior in the plane (Ω_m, β_1), (B_0, β_1) and (s, β_1). The grey and red contours show the posteriors from combined data set of *Planck* and growth rate measurements. The red contours are likelihood while evaluating the growth rate at an effective k ($\beta_1 < 1.010$), whereas grey contours are for the case when we use an effective growth rate, averaged over the scales used in the actual $f\sigma_8$ measurement ($\beta_1 < 1.010$). The green contour is combined constraint from *Planck* and eCMASS ($\beta_1 < 1.013$). Finally, the blue contours show the posterior from combined data of *Planck*, eCMASS and growth rate ($\beta_1 < 1.008$). We obtain the following joint constraint on the three Chameleon parameters: $\beta_1 < 1.008$, $B_0 < 1.0$ and $2.27 < s < 4$. While the constraints on the length-scale of the scalar field, B_0 and s are very broad, the one on the coupling, β_1, is very strong and predicts $\beta_1 = 1$ to 0.8 per cent, bringing μ to its GR value. As we already discussed for the scalar–tensor case, the discrepancy in the strength of these constraints is due to the fact that data prefer values of the coupling constant close to 1, for which the time and scale dependences of (μ, $\gamma_{\rm slip}$) become negligible. This is even more the case for Chameleon models, where the theoretical prior forces $\beta_1 > 1$, which corresponds to enhanced growth, and data consequently require very small values for this coupling, pushing μ very close to its GR value.

We have also looked at the extended Chameleon model where we allow β_1 to be less than 1 following previous analysis of this model. Fig. 11 shows the two-dimensional posterior in the plane (Ω_m, β_1). The red contours are likelihood while evaluating the growth rate at an effective k ($\beta_1 = 0.940 \pm 0.032$), whereas grey contours are for the case when we use an effective growth rate, averaged over the scales used in the actual $f\sigma_8$ measurement ($\beta_1 = 0.936 \pm 0.032$).

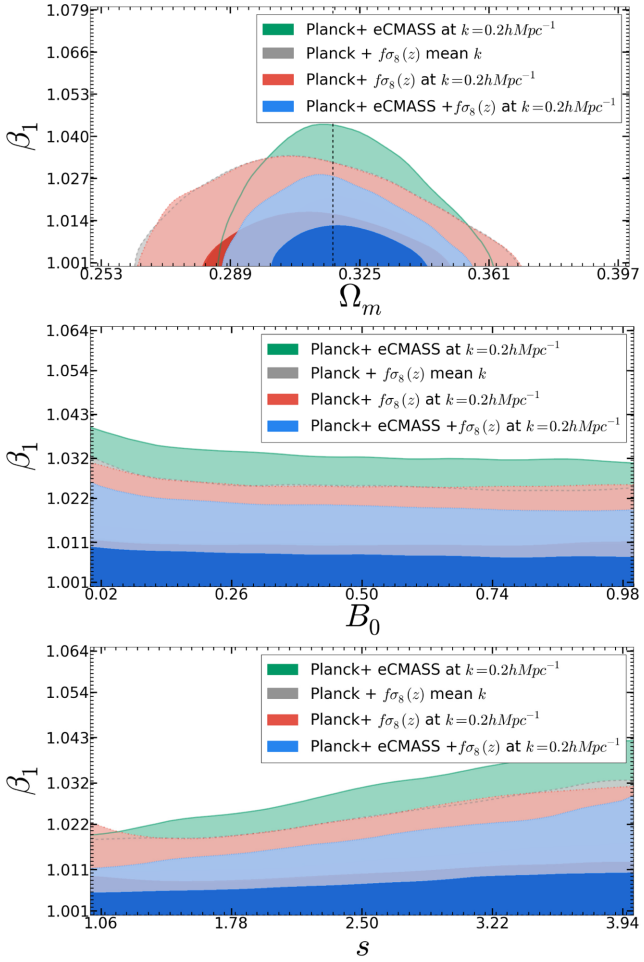

Figure 10. Chameleon theory: the two-dimensional posterior likelihood for Chameleon gravity. The green contour is the combined constraint from *Planck* and eCMASS ($\beta_1 < 1.013$). The grey contour is the combined constraint from *Planck* and $f\sigma_8(z)$ with averaged over k ($\beta_1 < 1.010$); the red contour is the combined constraint from *Planck* and $f\sigma_8(z)$ at effective $k = 0.2\,h$ Mpc^{-1} ($\beta_1 < 1.010$). The blue contour represents results from the combination of *Planck*, eCMASS and $f\sigma_8(z)$ ($\beta_1 < 1.008$).

The green contour is combined constraint from *Planck* and eCMASS ($\beta_1 = 0.932 \pm 0.04$). Finally, the blue contours show the posterior from combined data of *Planck*, eCMASS and growth rate ($\beta_1 = 0.932 \pm 0.031$). We obtain the following joint constraint on the three eChameleon parameters: $\beta_1 = 0.932 \pm 0.031$, $B_0 < 0.613$ and $2.69 < s < 4$. Like in the more general scalar–tensor case, while the constraints on the length-scale of the scalar field, B_0 and s are very broad, the one on the coupling, β_1, is a huge improvement on the previous constraint of $\beta_1 = 1.3 \pm 0.25$ (19.2 per cent measurement) using *WMAP* CMB, SNe and ISW data set (Hojjati et al. 2011). Let us notice that when we constrain jointly the three eChameleon parameters, data select a region in the parameter space which corresponds to $\beta_1 < 1$, i.e. to suppressed growth. This region excludes standard Chameleon models, including $f(R)$ theories, for which $\beta_1 > 1$ and the growth is enhanced. After all, as we have seen above and will see in the next section, the same data place very stringent constraints on Chameleon and $f(R)$ models, forcing them to be very close to ΛCDM (see Figs 11 and 12). Hence, the combination of data sets that we employ favours models with a suppressed growth rate, which adopting the BZ parametrization can be obtained with $\beta_1 < 1$; a suppressed growth was favoured also

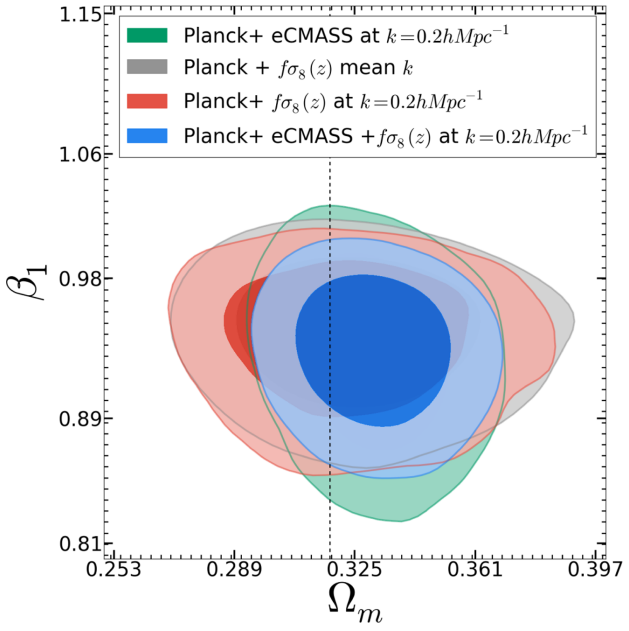

Figure 11. eChameleon theory: the two-dimensional posterior likelihood of β_1 and Ω_m for extended Chameleon gravity. The green contour is the combined constraint from *Planck* and eCMASS ($\beta_1 = 0.932 \pm 0.04$). The grey contour is the combined constraint from *Planck* and $f\sigma_8(z)$ with averaged over k ($\beta_1 = 0.940 \pm 0.032$); red contour is combined constraint from *Planck* and $f\sigma_8(z)$ at effective $k = 0.2\,h$ Mpc^{-1} ($\beta_1 = 0.936 \pm 0.032$). The blue contour represents results from the combination of *Planck*, $f\sigma_8(z)$ and eCMASS ($\beta_1 = 0.932 \pm 0.031$).

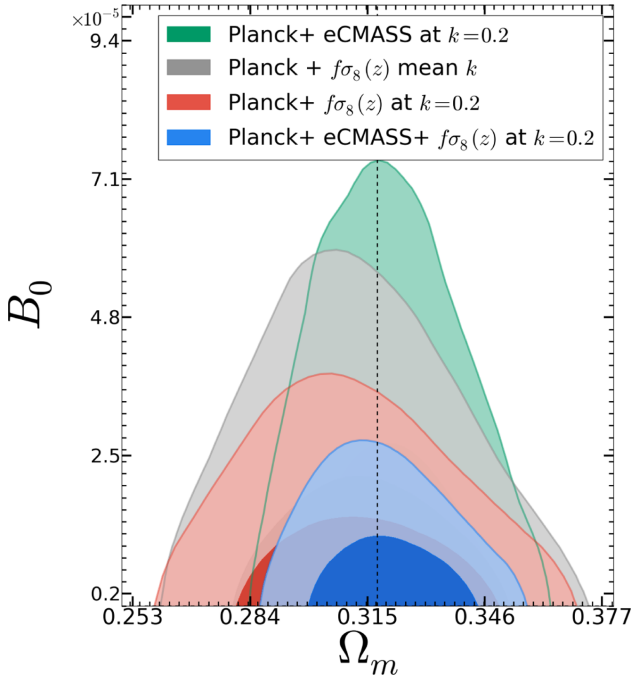

Figure 12. $f(R)$ gravity: the two-dimensional posterior likelihood of B_0 and Ω_m for $f(R)$ gravity. The green contour is combined constraint from *Planck* and eCMASS ($B_0 < 3.43 \times 10^{-5}$). The grey contour is the combined constraint from *Planck* and $f\sigma_8(z)$ with averaged over k ($B_0 < 2.77 \times 10^{-5}$); the red contour is the combined constraint from *Planck* and $f\sigma_8(z)$ at effective $k = 0.2\,h$ Mpc^{-1} ($B_0 < 1.89 \times 10^{-5}$). The blue contour represents results from the combination of *Planck*, $f\sigma_8(z)$ and eCMASS ($B_0 < 1.36 \times 10^{-5}$).

by the data set used in Planck Collaboration (2015b), although in that case the authors employed a time-dependent parametrization. Theoretically viable scalar–tensor models with a suppressed growth are discussed in Perenon et al. (2015), where they are analysed via a scale-independent parametrization in the effective field theory language.

6.7 *f*(*R*) theory

We consider one-parameter (B_0) model of $f(R)$ gravity. The parameter B_0 parametrizes the deviation from ΛCDM. The model approaches GR when B_0 is zero. Similar to Chameleon theory, $f(R)$ gravity predicts a scale-dependent growth rate ($f\sigma_8(k, z)$). Fig. 12 shows the two-dimensional posterior in B_0 and Ω_m plane. The green contour is combined constraint from *Planck* and eCMASS ($B_0 < 3.43 \times 10^{-5}$). The grey and red contours show posterior from combined data set of *Planck* and growth rate measurements. The red contours are likelihood while evaluating the growth rate at an effective k ($B_0 < 1.89 \times 10^{-5}$), whereas grey contours are for the case when we use effective growth rate, which is averaged over scales used in the actual $f\sigma_8$ measurements ($B_0 < 2.77 \times 10^{-5}$). The blue contours show the posterior from combined data of *Planck*, eCMASS and growth rate ($B_0 < 1.36 \times 10^{-5}$). We obtained $B_0 < 1.36 \times 10^{-5}$ (1σ C.L.), which is an improvement by a factor of 4 on the most recent constraint from large-scale structure of $B_0 = 5.7 \times 10^{-5}$ (1σ C.L.; Xu 2015). Our constraint is competitive with the constraint from Solar system tests and clusters (Hu & Sawicki 2007; Schmidt, Vikhlinin & Hu 2009; Cataneo et al. 2015).

6.8 Growth index (γ) parametrization

The standard cosmological model, based on GR, predicts a precise value for the growth factor in the linear regime, i.e. $f = \Omega_m^{0.55}$. In order to test deviations from GR, we have parametrized the growth factor using growth index γ (Linder & Cahn 2008) as $f = \Omega_m^{\gamma}$. The marginalized two-dimensional likelihood for Ω_m and γ is shown in Fig. 13. The grey contour is combined constraint from *Planck* and eCMASS ($\gamma = 0.477 \pm 0.096$). The red contours show the constraint obtained using *Planck* and $f\sigma_8(z)$ measurement ($\gamma = 0.595 \pm 0.079$) and the blue contours are for combined data set of *Planck* with $f\sigma_8(z)$ and eCMASS ($\gamma = 0.612 \pm 0.072$). We have obtained $\gamma = 0.612 \pm 0.072$ (11.7 per cent measurement) completely consistent with the GR prediction.

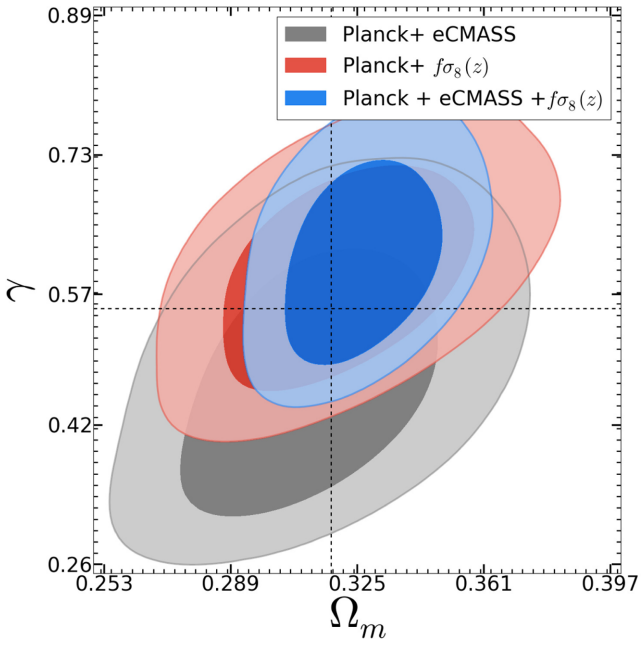

Figure 13. Growth index (γ): the two-dimensional posterior likelihood of γ and Ω_m for growth index parametrization. The grey contour is the combined constraint from *Planck* and eCMASS ($\gamma = 0.477 \pm 0.096$). The red contour is the combined constraint from *Planck* and $f\sigma_8(z)$ ($\gamma = 0.595 \pm 0.079$). The blue contour represents results from the combination of *Planck*, $f\sigma_8(z)$ and eCMASS ($\gamma = 0.612 \pm 0.072$).

7 DISCUSSION

We have constrained the parameters of the standard cosmological model, ΛCDM, as well as those of various extensions using the current measurements of growth rate between redshift 0.06 and 0.83 (Fig. 4), eCMASS and *Planck* 2013. We have been careful with several important details while combining results from various surveys and different cosmologies of measurements. We have first showed that the standard ΛCDM parameter space has a consistent posterior, independent of the model considered except for Chameleon gravity. Next, we focused on each model and analysed the constraint on its extension parameters. As for the standard model, ΛCDM, using the growth factor we do not improve constraints on any of its parameters because the growth rate is already highly constrained with *Planck* measurement for the standard model of cosmology. It is impressive to notice that ΛCDM, without any extra parameter, is completely consistent with the measurements of $f\sigma_8$ from very different galaxy types and redshifts. In the case of the extension where the DE equation of state is constant but free to vary, wCDM, we obtain $w_0 = -0.87 \pm 0.077$ (8.8 per cent measurement). This is a 3.7 times improvement on the precision compared to *Planck*-only measurement $w = -1.27 \pm 0.42$ (33 per cent measurement) and comparable to the 8 per cent measurement of Samushia et al. (2012). Our measurement prefers $w < -1$ at the 1σ level. We have also noticed that the growth rate and BAO have slightly different degeneracy for wCDM. This shows the potential to improve the constraint on w by combining the growth rate and BAO measurements from a range of galaxy redshift surveys. However, one difficulty in doing so is to model the correlation between the measurement of growth rate and BAO.

We also report one of the best measurements on the parameters of the model with a time-dependent equation of state, w_0w_aCDM. We have measured $w_0 = -0.94 \pm 0.17$ (18 per cent measurement) and $1 + w_a = 1.16 \pm 0.36$ (31 per cent measurement). This represents a significant improvement on w_a compared to all other measurements (Aubourg et al. 2015; Planck Collaboration I 2014a). The measurements of $f\sigma_8$, H and D_A in eCMASS help to constrain ΛCDM parameters, while the evolution of the growth rate over a large redshift range, obtained through measurements of $f\sigma_8(z)$ at multiple redshifts, improves the constraint on evolving DE. This hints at the potential of using combined growth rate and anisotropic BAO as a function of redshifts, when future surveys like eBOSS and *Euclid* (Laureijs et al. 2011) will provide much stronger growth rate and BAO constraints at much higher redshifts. We have also looked at the possibility of a non-zero curvature for the universe, $o\Lambda$CDM, finding $1 + \Omega_k = 0.9976 \pm 0.0032$ (0.3 per cent measurement), which is the same as the best constraint reported in Samushia et al. (2012). We notice that the optical depth (τ) and amplitude of scalar power spectrum (A_s) are relatively low for $o\Lambda$CDM, which predicts smaller redshift of reionization ($z_{re} = 7.20 \pm 2.81$) but is above the

lower limit observed through Lyman α forest observations (Becker et al. 2001).

We have also looked at some of the popular modifications of gravity and found no significant deviations from GR using growth rate and *Planck* 2013 measurement. We have investigated general scalar–tensor theories under the parametrization introduced in Bertschinger & Zukin (2008), constraining the corresponding five parameters. We have found constraints on the two coupling parameters ($\beta_1 = 1.23 \pm 0.29$, $\beta_2 = 0.93 \pm 0.44$), while the posterior of other three parameters was largely non-constraining. We then restricted to the subset of Chameleon theories, for which only three parameters are needed. While imposing a theoretical bound of $\beta_1 > 1$, we constrained the coupling of Chameleon theories to $\beta_1 < 1.008$ (1σ C.L.), while jointly varying the remaining two free parameters that describe the length-scale of the scalar degree of freedom, $\{B_0, s\}$. While the latter are loosely constrained by data, the constraint on the coupling is quite stringent. We also explored an extension of Chameleon models, which we dubbed eChameleon, where we let the coupling β_1 vary within the range [0, 2]. Also in this case, data place a stringent bound on the coupling, while loosely constraining $\{B_0, s\}$. Interestingly, for this case data select a region where $\beta_1 < 1$, with the bound $\beta_1 = 0.932 \pm 0.031$; the latter corresponds to a region of the parameter space for which growth is suppressed. This improves significantly over previous analysis, e.g. the bound $\beta_1 = 1.3 \pm 0.25$ (19.2 per cent measurement) obtained in Hojjati et al. (2011) using *WMAP* CMB, SNe and ISW data set. This excludes standard Chameleon models, including $f(R)$ theories, for which $\beta_1 > 1$ and the growth is enhanced. After all, the same data place very stringent constraints on the latter models, forcing them to be very close to ΛCDM (see Figs 11 and 12). We also notice that the optical depth (τ) and amplitude of scalar power spectrum (A_s) are higher for eChameleon gravity. This predicts higher redshift of reionization ($z_{re} = 14.43 \pm 3.77$) and higher growth. In such a situation, the only way in which the model can align itself with the measured $f\sigma_8$ is by choosing a smaller coupling parameter (β_1). We have placed very stringent bounds on $f(R)$ models with a ΛCDM background, constraining their only free parameter to be $B_0 < 1.36 \times 10^{-5}$ (1σ C.L.). This is competitive with the constraint from Solar system tests and clusters (Hu & Sawicki 2007; Schmidt et al. 2009; Cataneo et al. 2015) and other cosmological measurements (Dossett, Hu & Parkinson 2014; Raveri et al. 2014; Planck Collaboration et al. 2015b; Xu 2015).

Finally, we have analysed the growth index parametrization of the growth rate, measuring $\gamma = 0.612 \pm 0.072$ (11.7 per cent measurement), which is completely consistent with the GR prediction. This is a slight improvement on the 16 per cent measurement of Samushia et al. (2014). We also note that our measurement of growth index is slightly less precise than current best measurement $\gamma = 0.665 \pm 0.0669$ (10 per cent measurement; Johnson et al. 2015) using combination of galaxy power spectrum, velocity power spectrum, Type Ia SNe, the CMB, CMB lensing and the temperature-galaxy cross-correlation.

It is remarkable to notice that even after allowing many different kinds of degrees of freedom, our analysis shows that everything is consistent with vanilla ΛCDM cosmology and general theory of relativity.

ACKNOWLEDGEMENTS

We would like to thank Martin White and Eric Linder for providing us many important suggestions on the draft of our paper and discussing various theoretical and observational details. We also want to thank Lado Samushia for feedback on the clarity of the text. We would also like to thank Mark Trodden and Levon Pogosian for reading through the draft of our paper. SA and SH are supported by NASA grant NASA 12-EUCLID11-0004 and NSF AST1412966 for this work. AS acknowledges support from the Netherlands Organisation for Scientific Research (NWO/OCW), and also from the D-ITP consortium, a programme of the Netherlands Organisation for Scientific Research (NWO) that is funded by the Dutch Ministry of Education, Culture and Science (OCW). This work made extensive use of the NASA Astrophysics Data System and of the `astro-ph` preprint archive at `arXiv.org`.

REFERENCES

Alam S. et al., 2015a, ApJS, 219, 12
Alam S., Ho S., Vargas Magaña M., Schneider D. P., 2015b, MNRAS, 453, 1754
Alcock C., Paczynski B., 1979, Nature, 281, 358
Amendola L., Kunz M., Motta M., Saltas I. D., Sawicki I., 2013, Phys. Rev. D, 87, 023501
Anderson L. et al., 2014a, MNRAS, 439, 83
Anderson L. et al., 2014b, MNRAS, 441, 24
Aubourg E. et al., 2015, Phys. Rev. D, 92, 123516
Becker R. H. et al., 2001, AJ, 122, 2850
Bennett C. L. et al., 2013, ApJS, 208, 20
Bertschinger E., Zukin P., 2008, Phys. Rev. D, 78, 024015
Beutler F. et al., 2012, MNRAS, 423, 3430
Blake C. et al., 2011a, MNRAS, 415, 2876
Blake C. et al., 2011b, MNRAS, 418, 1707
Carlson J., Reid B., White M., 2013, MNRAS, 429, 1674
Carroll S. M., 2001, Living Rev. Relativ., 4, 1
Cataneo M. et al., 2015, Phys. Rev. D, 92, 044009
Chevallier M., Polarski D., 2001, Int. J. Mod. Phys. D, 10, 213
Clifton T., Ferreira P. G., Padilla A., Skordis C., 2012, Phys. Rep., 513, 1
Cole S. et al., 2005, MNRAS, 362, 505
Colless M. et al., 2003, preprint (astro-ph/0306581)
Conley A. et al., 2011, ApJS, 192, 1
Copeland E. J., Sami M., Tsujikawa S., 2006, Int. J. Mod. Phys. D, 15, 1753
Davis M., Peebles P. J. E., 1983, ApJ, 267, 465
Dawson K. S. et al., 2013, AJ, 145, 10
de Felice A., Mukohyama S., Tsujikawa S., 2010, Phys. Rev. D, 82, 023524
de la Torre S. et al., 2013, A&A, 557, A54
de Putter R., Linder E. V., 2008, J. Cosmol. Astropart. Phys., 10, 42
Di Valentino E., Melchiorri A., Salvatelli V., Silvestri A., 2012, Phys. Rev. D, 86, 063517
Dossett J., Hu B., Parkinson D., 2014, J. Cosmol. Astropart. Phys., 3, 46
Einstein A., 1915, Sitzungsberichte der Preussischen Akademie der Wissenschaften zu Berlin, 844
Eisenstein D. J. et al., 2005, ApJ, 633, 560
Eisenstein D. J. et al., 2011, AJ, 142, 72
Fang W., Hu W., Lewis A., 2008, Phys. Rev. D, 78, 087303
Goobar A., Leibundgut B., 2011, Annu. Rev. Nucl. Part. Sci., 61, 251
Hinshaw G. et al., 2013, ApJS, 208, 19
Hojjati A., Pogosian L., Zhao G.-B., 2011, J. Cosmol. Astropart. Phys., 8, 5
Hojjati A., Pogosian L., Silvestri A., Talbot S., 2012, Phys. Rev. D, 86, 123503
Hu W., Sawicki I., 2007, Phys. Rev. D, 76, 064004
Hu B., Raveri M., Frusciante N., Silvestri A., 2014, Phys. Rev. D, 89, 103530
Huterer D., Turner M. S., 1999, Phys. Rev. D, 60, 081301
Huterer D. et al., 2015, Astropart. Phys., 63, 23
Hütsi G., 2006, A&A, 446, 43
Jennings E., Baugh C. M., Pascoli S., 2011, MNRAS, 410, 2081
Johnson A., Blake C., Dossett J., Koda J., Parkinson D., Joudaki S., 2015, preprint (arXiv:1504.06885)
Jones D. H. et al., 2009, MNRAS, 399, 683
Kaiser N., 1987, MNRAS, 227, 1

Linder E. V., Cahn R. N., 2007, Astropart. Phys., 28, 481
Kazin E. A. et al., 2010, ApJ, 710, 1444
Laureijs R. et al., 2011, preprint (arXiv:1110.3193)
Lewis A., Bridle S., 2002, Phys. Rev. D, 66, 103511
Linder E. V., 2003, Phys. Rev. Lett., 90, 091301
Linder E. V., 2005, Phys. Rev. D, 72, 043529
Linder E. V., Cahn R. N., 2007, Astropart. Phys., 28, 481
Peebles P. J. E., 1980, The Large-Scale Structure of the Universe. Princeton Univ. Press, Princeton, NJ
Percival W. J. et al., 2004, MNRAS, 353, 1201
Percival W. J. et al., 2010, MNRAS, 401, 2148
Perenon L., Piazza F., Marinoni C., Hui L., 2015, J. Cosmol. Astropart. Phys., 11, 029
Perlmutter S., Schmidt B. P., 2003, in Weiler K., ed., Lecture Notes in Physics, Vol. 598, Supernovae and Gamma-Ray Bursters. Springer-Verlag, Berlin
Perlmutter S. et al., 1999, ApJ, 517, 565
Planck Collaboration I, 2014a, A&A, 571, A1
Planck Collaboration XV, 2014b, A&A, 571, A15
Planck Collaboration XVI, 2014c, A&A, 571, A16
Planck Collaboration XIII, 2015a, preprint (arXiv:1502.01589)
Planck Collaboration XIV, 2015b, preprint (arXiv:1502.01590)
Pogosian L., Silvestri A., 2008, Phys. Rev. D, 77, 023503
Raveri M., Hu B., Frusciante N., Silvestri A., 2014, Phys. Rev. D, 90, 043513
Reid B. A. et al., 2010, MNRAS, 404, 60
Reid B. et al., 2016, MNRAS, 455, 1553
Riess A. G. et al., 1998, AJ, 116, 1009
Rodney S. A. et al., 2014, AJ, 148, 13
Samushia L., Percival W. J., Raccanelli A., 2012, MNRAS, 420, 2102
Samushia L. et al., 2014, MNRAS, 439, 3504
Schmidt F., Vikhlinin A., Hu W., 2009, Phys. Rev. D, 80, 083505
Silvestri A., Trodden M., 2009, Rep. Prog. Phys., 72, 096901
Silvestri A., Pogosian L., Buniy R. V., 2013, Phys. Rev. D, 87, 104015
Song Y.-S., Hu W., Sawicki I., 2007, Phys. Rev. D, 75, 044004
Suzuki N. et al., 2012, ApJ, 746, 85
Wang L., Steinhardt P. J., 1998, ApJ, 508, 483
Wang L., Reid B., White M., 2014, MNRAS, 437, 588
Weinberg S., 1989, Rev. Mod. Phys., 61, 1
Xu L., 2015, Phys. Rev. D, 91, 063008
Zhao G.-B., Pogosian L., Silvestri A., Zylberberg J., 2009, Phys. Rev. D, 79, 083513

This paper has been typeset from a TEX/LATEX file prepared by the author.